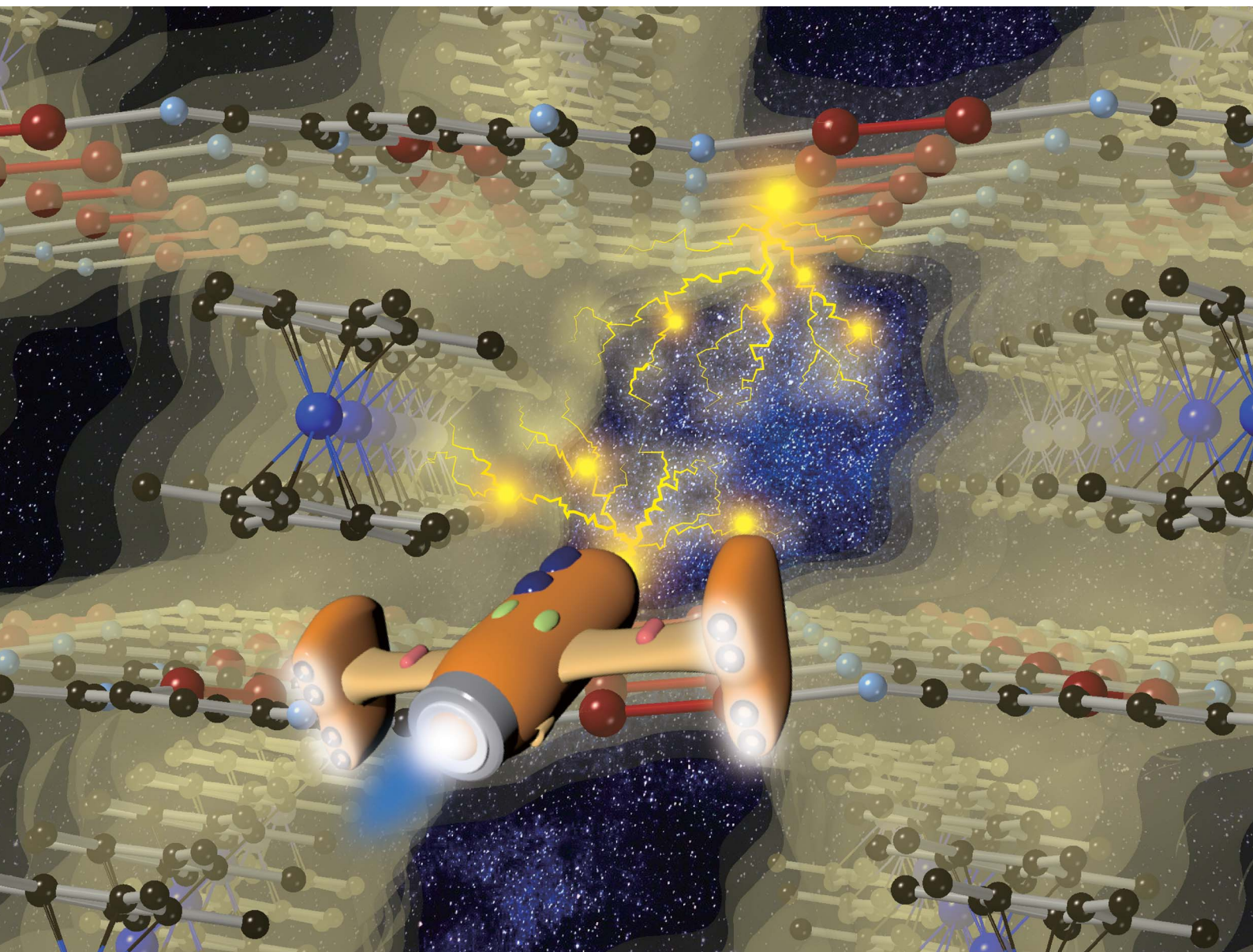


Chemical Science

Volume 14
Number 4
28 January 2023
Pages 725–1028

rsc.li/chemical-science



ISSN 2041-6539

EDGE ARTICLE

Hitoshi Miyasaka *et al.*
Inter-layer magnetic tuning by gas adsorption in π -stacked
pillared-layer framework magnets

Cite this: *Chem. Sci.*, 2023, 14, 791

All publication charges for this article have been paid for by the Royal Society of Chemistry

Inter-layer magnetic tuning by gas adsorption in π -stacked pillared-layer framework magnets†

Wataru Kosaka,^a Honoka Nemoto,^b Kohei Nagano,^b Shogo Kawaguchi,^c Kuniyoshi Sugimoto^{cd} and Hitoshi Miyasaka^{ab*}

Magnetism of layered magnets depends on the inter-layer through-space magnetic interactions (J_{NNNI}). Using guest sorption to address inter-layer pores in bulk-layered magnets is an efficient approach to magnetism control because the guest-delicate inter-layer distance (l_{trans}) is a variable parameter for modulating J_{NNNI} . Herein, we demonstrated magnetic changes induced by the adsorption of CO_2 , N_2 , and O_2 gases in various isostructural layered magnets with a π -stacked pillared-layer framework, $[\text{MCp}_2^*]\{\{\text{Ru}_2(2,3,5,6\text{-F}_4\text{PhCO}_2)_4\}_2(\text{TCNQ})\}$, ($M = \text{Co}$, **1**, Fe , **2**, Cr , **3**; $\text{Cp}^* = \eta^5\text{-C}_5\text{Me}_5$; $2,3,5,6\text{-F}_4\text{PhCO}_2^- = 2,3,5,6\text{-tetrafluorobenzoate}$; $\text{TCNQ} = 7,7,8,8\text{-tetracyano-}p\text{-quinodimethane}$). Each compound had almost identical adsorption capability for the three types of gases; only CO_2 adsorption was found to have a gated profile. A breathing-like structural modulation involving the extension of l_{trans} occurred after the insertion of gases into the isolated pores between the $[\text{Ru}_2]_2\text{-TCNQ}$ ferrimagnetic layers, which is more significant for CO_2 than for O_2 and N_2 , due to the CO_2 -gated transition. While adsorbent **1** with $M = \text{Co}$ ($S = 0$) was an antiferromagnet with $T_N = 75$ K, $\mathbf{1} \supset \text{CO}_2$ was a ferrimagnet with $T_C = 76$ K, whereas $\mathbf{1} \supset \text{N}_2$ and $\mathbf{1} \supset \text{O}_2$ were antiferromagnets with $T_N = 68$ K. The guest-insertion effect was similarly confirmed in **2** and **3**, and was characteristically dependent on the type of sandwiched spin in $[\text{MCp}_2^*]^+$ as $M = \text{Fe}$ ($S = 1/2$) and Cr ($S = 3/2$), respectively. This study reveals that common gases such as CO_2 , O_2 , and N_2 can serve as crucial triggers for the change in magnetism as a function of variable parameter l_{trans} .

Received 17th November 2022
Accepted 24th December 2022

DOI: 10.1039/d2sc06337a

rsc.li/chemical-science

Introduction

The coupling of porosity-related capacity and magnetism is a fascinating approach toward the design of functional porous materials based on metal-organic frameworks (MOFs) and porous coordination polymers.^{1–7} Moreover, the focal points in the investigation of porosity and magnetism are fundamentally different. While the utilization of well-ordered pores of materials focuses on functionalizing the space bounded by frameworks,^{8–15} the concept of magnetism has mainly been utilized as a framework design to control spin ordering through the strong integration of paramagnetic spins through frontier

orbitals of frameworks; this concept has also been applied to the design of magnetically conjugated paramagnetic frameworks.^{16–21} In contrast, the magnetism of low-dimensional framework systems such as layered MOF (LMOF) systems has gained considerable attention. In LMOF systems, inter-layer interactions, *i.e.*, through-space interactions, play a crucial role in tuning long-range magnetic ordering;^{22–26} hence, the absence of inter-layer interactions is considered evidence of mono-layer magnets.^{27–31} Therefore, magnetic LMOFs are a good platform for investigating guest effects in magnetism. Switching magnetic ground states, *i.e.*, the magnetic phases, as a function of the type of intercalated guest molecules between layers is a challenging subject.^{32,33} Indeed, guest-induced magnetic modifications of several magnetic LMOFs (bulk phase) have been reported so far, which are roughly categorized into four groups from the viewpoint of mechanism (Fig. 1a–d);³² (i) structural modification including crystal-amorphous change (Fig. 1a);^{34–40} (ii) induction of electron transfer (ET) in the frameworks (Fig. 1b);^{41–45} (iii) magnetic mediation by paramagnetic guest molecules (Fig. 1c);⁴⁶ and (iv) host-guest charge transfer or ET (Fig. 1d).⁴⁷ The modulation of the layer-stacking mode through guest adsorption/desorption is the subject of mechanism (i).^{48–52} However, the guest-induced variation in the magnetic ground state following mechanism (i) is only known

^aInstitute for Materials Research, Tohoku University, 2-1-1 Katahira, Aoba-ku, Sendai 980-8577, Japan. E-mail: miyasaka@imr.tohoku.ac.jp

^bDepartment of Chemistry, Graduate School of Science, Tohoku University, 6-3 Aramaki-Aza-Aoba, Aoba-ku, Sendai 980-8578, Japan

^cDiffraction & Scattering Division, Japan Synchrotron Radiation Research Institute, 1-1-1 Kouto, Sayo-cho, Sayo-gun, Hyogo 679-5198, Japan

^dDepartment of Chemistry, Kindai University, 3-4-1 Kowakae, Higashi-Osaka, Osaka 577-8502, Japan

† Electronic supplementary information (ESI) available: Synthesis, crystallography, and characterization details (PDF). CCDC 2219754–2219756. For ESI and crystallographic data in CIF or other electronic format see DOI: <https://doi.org/10.1039/d2sc06337a>



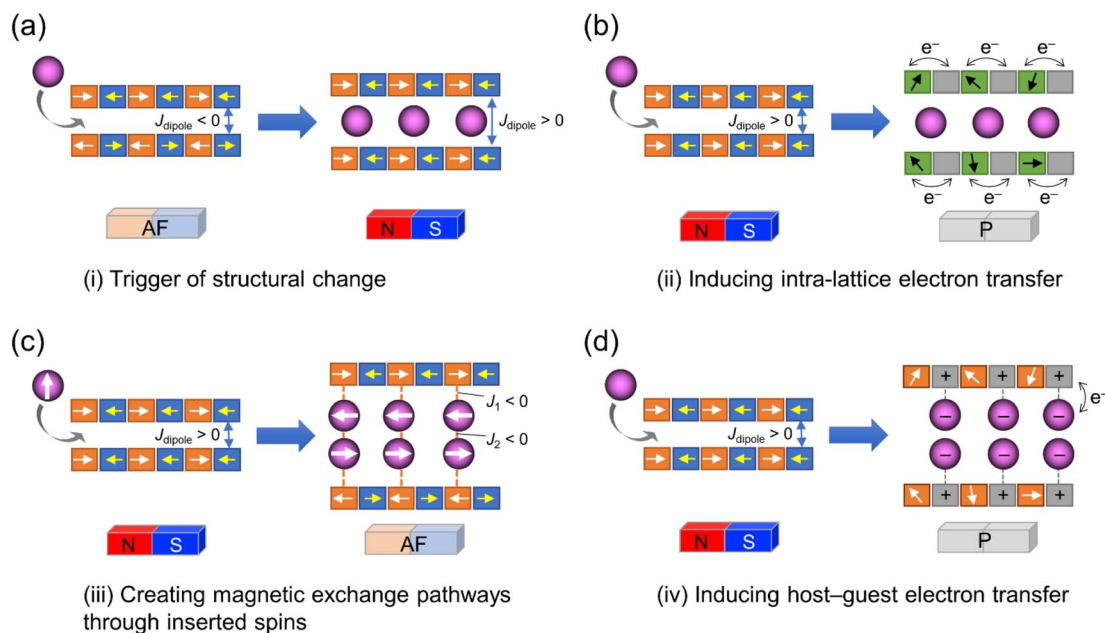


Fig. 1 Four mechanisms for ON/OFF switching of layered magnets by guest adsorption. (a) Adsorption-induced structural change. (b) Adsorption-induced intra-lattice ET. (c) Creating magnetic exchange pathways through inserted spins. (d) Adsorption-induced host-guest ET.

in a few cases of magnetic LMOFs,^{34–40} and examples driven by common gases such as carbon dioxide (CO₂), oxygen (O₂), and nitrogen (N₂) have not yet been reported.

Herein, we report the gas-selective magnetic responsivity of a family of isostructural π -stacked pillared-layer compounds, [MCP₂^{*}][{Ru₂^{II,II}(2,3,5,6-F₄PhCO₂)₄]₂(TCNQ)] (M = Co, **1**; Fe, **2**; Cr, **3**; Cp^{*} = η -C₅Me₅; 2,3,5,6-F₄PhCO₂⁻ = 2,3,5,6-tetrafluorobenzoate; TCNQ = 7,7,8,8-tetracyano-*p*-quinodimethane) (Fig. 2).^{53,54} These compounds are composed of ferrimagnetic layers [{Ru₂^{II,II}(2,3,5,6-F₄PhCO₂)₄]₂(TCNQ)]⁻ and sandwiched dodecamethylmetallocenium [MCP₂^{*}]⁺ in a π -stacking columnar mode as [⋯{TCNQ}⋯{MCP₂^{*}}⋯] (Fig. 2a),^{55–60} which are denoted as π -PLFs. The compounds have almost identical gas adsorption capabilities for common gases such as CO₂ (4–6 mol mol⁻¹ at 195 K), O₂ (3–5 mol mol⁻¹ at 120 K), and N₂ (1–2 mol mol⁻¹ at 120 K). However, they undergo a breathing-like structural modulation involving an extension of the inter-layer distance, which is more significant after the adsorption of CO₂ than that of O₂ and N₂. Thereby, **1** with [CoCp₂^{*}]⁺ (*S* = 0), which is an antiferromagnet (AF) with *T*_N = 75 K (*T*_N = Néel temperature),⁵⁴ undergoes a change in the magnetic ground state to a ferrimagnet (F) with *T*_C = 76 K (*T*_C = Curie temperature) in **1**⊃CO₂, while maintains its antiferromagnetic state in **1**⊃O₂ and **1**⊃N₂ although their *T*_N is shifted to a lower temperature of 68 K than that in **1**. The effect of guest insertion of CO₂, O₂, and N₂ is similarly confirmed in **2** and **3**, but is characteristically dependent on the type of the sandwiched spin in [MCP₂^{*}]⁺ with M = Fe (*S* = 1/2) and Cr (*S* = 3/2), respectively.⁵⁴ As a typical prototype of mechanism (i), this work demonstrates that inter-layer magnetic interactions closely associated with inter-layer distance can tune the coupling of ubiquitous gas adsorption capability and magnetism in magnetic LMOFs.

Results and discussion

Gas adsorption properties of 1–3

Compounds **1–3** were synthesized according to a previous report.⁵⁴ Fig. 2b and c display the packing views of **1** as revealed by Rietveld analysis. In the π -PLF structures of **1–3**, the lattice constant *a* corresponds to the inter-unit distance between two-dimensional [Ru₂]₂-TCNQ layers, also known as the translational distance, *l*_{trans}, which was found to be 10.3795(5) Å (100 K), 10.2874(6) Å (135 K), and 10.5456(2) Å (120 K) for **1**, **2**, and **3**, respectively (Fig. 2c). As shown in the Connolly surface views in Fig. 2b and c, small pores were present in **1** as isolated cavities surrounded by layers and [MCP₂^{*}]⁺ cations.

Each compound adsorbed different amounts of CO₂, O₂, and N₂, but their adsorption/desorption isotherms were very similar (Fig. 3). Only **3** adsorbed slightly larger amounts of gases than **1** and **2**, which could be due to its somewhat larger void space than those of **1** and **2** as realized in their pristine solvated compounds.⁵⁴ At 99 kPa (= *P*_{gas}), the amounts of adsorbed CO₂ (195 K), O₂ (120 K), and N₂ (120 K) were 2.1 mmol g⁻¹ (5.3 mol mol⁻¹), 1.2 mmol g⁻¹ (3.1 mol mol⁻¹), and 0.3 mmol g⁻¹ (0.8 mol mol⁻¹) for **1**; 1.9 mmol g⁻¹ (4.8 mol mol⁻¹), 1.2 mmol g⁻¹ (2.9 mol mol⁻¹), and 0.2 mmol g⁻¹ (0.6 mol mol⁻¹) for **2**; 2.5 mmol g⁻¹ (6.1 mol mol⁻¹), 1.9 mmol g⁻¹ (4.8 mol mol⁻¹), and 0.6 mmol g⁻¹ (1.4 mol mol⁻¹) for **3**, respectively. The amount of O₂ adsorbed at 90 K was less than that adsorbed at 120 K. This could be because the adsorption is kinetically difficult at lower temperatures, such as 90 K, because the structure becomes more rigid.^{43,46,61–63} A small step was observed in the adsorption isotherm of CO₂ at *P*_{CO₂} = 15–20 kPa for **1–3**, albeit much more remarkable for **1** (Fig. 3). Despite being small, this step was an important sign that indicated a significant structural change in the process of CO₂ adsorption (*vide infra*).



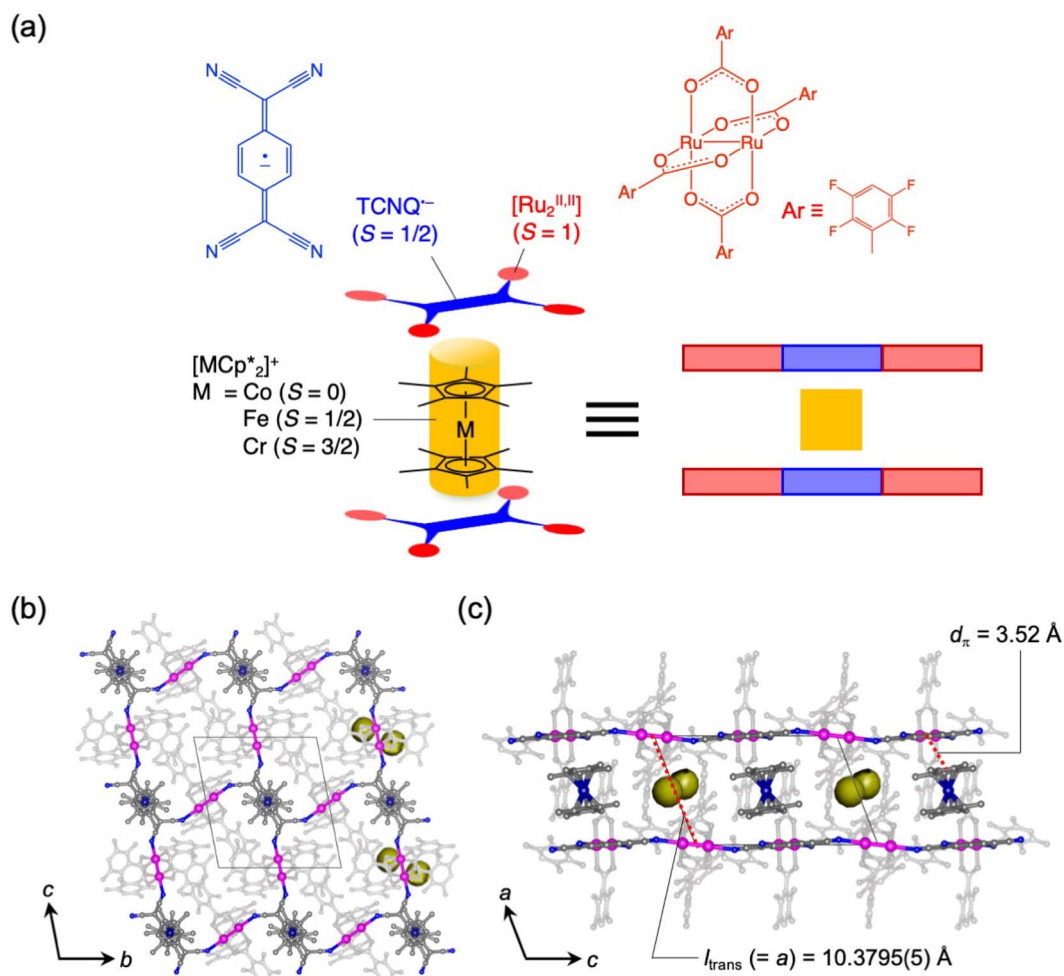


Fig. 2 Structural overview of the series of π -PLFs and representative **1**. (a) Schematic representation of the building units for the π -PLF. (b and c) Packing views of **1** projected along the a - and b -axes, respectively, where hydrogen atoms are omitted for clarity; C, N, Co, and Ru atoms are presented in gray, blue, navy, and purple, respectively; atoms of 2,3,5,6-F₄PhCO₂[−] ligands are depicted in pale gray for clarity; and Connolly surfaces of void space are shown in yellow.

Gas adsorption properties of 1–3

In situ powder X-ray diffraction (PXRD) was conducted to gain insights into the crystal structures under gas adsorption conditions. The CO₂-pressure dependence of the PXRD pattern

of **1** at 195 K is shown in Fig. 4a. A small but distinct peak shift was observed after P_{CO_2} was increased from 10 to 20 kPa, corresponding to the step-like anomaly in the CO₂ adsorption isotherm shown in Fig. 3a. The lattice constants obtained by Le

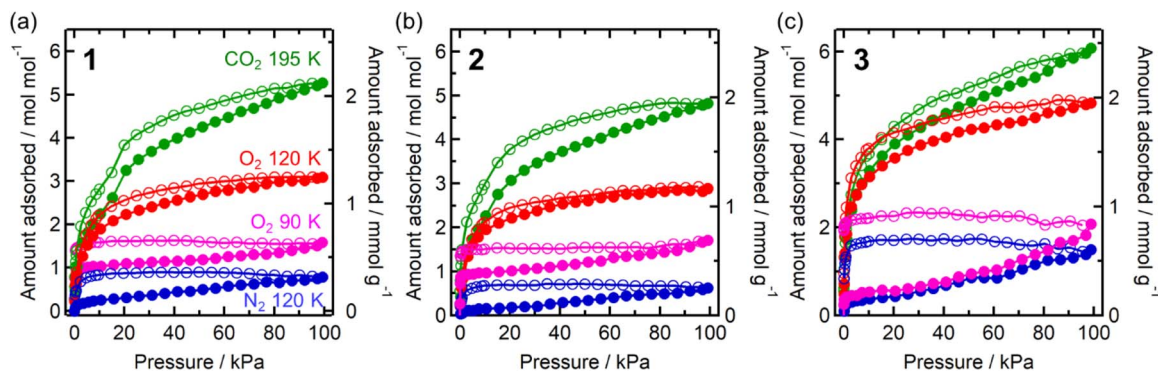


Fig. 3 Gas adsorption (closed) and desorption (open) isotherms of **1**–**3** (a–c, respectively) for CO₂ at 195 K (green), O₂ at 90 K (pink) and 120 K (red), and N₂ at 120 K (blue).



Bail or Rietveld analysis for each pattern are summarized in Table S1,[†] and the changes in the lattice constants a , b , and c relative to those for pristine **1** are shown in Fig. 4b. Upon increasing P_{CO_2} , the amount of adsorbed CO_2 and, consequently, the lattice constants increased. Significantly, the lattice constant a ($= l_{\text{trans}}$) increased non-linearly from 10.38 Å for pristine **1** (before introducing CO_2) at $P_{\text{CO}_2} \approx 10$ kPa, to 10.84 Å for $\mathbf{1} \supset \text{CO}_2$ at $P_{\text{CO}_2} = 100$ kPa (total of +4% increase). In contrast, the increasing ratios of lattice constants b and c were less than 1%.

The PXRD patterns obtained under vacuum and at $P_{\text{O}_2/\text{N}_2} = 100$ kPa at 120 K are shown in Fig. 4c, and the lattice constants obtained by Rietveld analysis are listed in Table S1.[†] The relative changes along the a -axis ($= l_{\text{trans}}$) are shown in Fig. 4d. No significant change was observed in the PXRD patterns of gas-dosed $\mathbf{1} \supset \text{O}_2$ and $\mathbf{1} \supset \text{N}_2$. In fact, the length of the a -axis of $\mathbf{1} \supset \text{O}_2$ and $\mathbf{1} \supset \text{N}_2$ at $P_{\text{O}_2/\text{N}_2} = 100$ kPa remained at 10.36 Å, which was comparable to that of pristine **1**.

The structures of gas-adsorbed $\mathbf{1} \supset \text{CO}_2$ at 195 K, $\mathbf{1} \supset \text{O}_2$ at 120 K, and $\mathbf{1} \supset \text{N}_2$ at 120 K were determined by Rietveld refinements using the corresponding PXRD patterns taken at $P_{\text{gas}} = 100$ kPa (Fig. 4e–j, Tables S1 and S2[†]), where the determined gas molecules are not displayed because of the inaccuracy of their local positions even in the Rietveld analysis. No significant difference was found in the frameworks of the gas-inserted phases ($\mathbf{1} \supset \text{gas}$) when compared to those of pristine **1**. Isolated gas-

accommodating cavities with volumes of 155, 103, and 97 Å³ were found in $\mathbf{1} \supset \text{CO}_2$, $\mathbf{1} \supset \text{O}_2$, and $\mathbf{1} \supset \text{N}_2$, respectively, located in the same position between the $[\text{Ru}_2]_2$ -TCNQ layers and between the $[\text{CoCp}_2^*]$ cations regardless of the type of gas (but the amount was different). Their sharing positions are displayed as Connolly surface views in Fig. 4e–j.⁵⁴ The π -stack distances (d_{π} ; see Fig. 2c), defined as the distance between the centers of the 6-membered ring of TCNQ and the 5-membered ring of $[\text{CoCp}_2^*]$, were found to be 3.76, 3.49, and 3.51 Å in $\mathbf{1} \supset \text{CO}_2$, $\mathbf{1} \supset \text{O}_2$, and $\mathbf{1} \supset \text{N}_2$, respectively. The values of d_{π} measured for $\mathbf{1} \supset \text{O}_2$ and $\mathbf{1} \supset \text{N}_2$ were very similar to that for **1** (3.52 Å), whereas the π -stack distance in $\mathbf{1} \supset \text{CO}_2$ was 0.24 Å larger than that in **1** ($\Delta d_{\pi} = 0.24$ Å). In fact, the change in l_{trans} between **1** and $\mathbf{1} \supset \text{CO}_2$ (0.46 Å) is near twice the value of Δd_{π} .

Infrared (IR) spectra were recorded for $\mathbf{1} \supset \text{CO}_2$, $\mathbf{1} \supset \text{O}_2$, and $\mathbf{1} \supset \text{N}_2$ at $P_{\text{gas}} = 100$ kPa and at 195, 120, and 120 K, respectively. The positions of the peaks corresponding to the $\text{C}\equiv\text{N}$ stretching mode observed for $\mathbf{1} \supset \text{CO}_2$, $\mathbf{1} \supset \text{O}_2$, and $\mathbf{1} \supset \text{N}_2$ remained unchanged compared to that for **1** (Fig. S2[†]), indicating no change in the electronic state after gas dosing.

Magnetic properties of **1** under gases

Adsorbent **1** (*i.e.*, pristine form) is an AF with $T_{\text{N}} = 75$ K (black plot in Fig. 5).⁵⁴ First, the behavior under a N_2 atmosphere, that is, $\mathbf{1} \supset \text{N}_2$, is described because **1** adsorbs only one molar equivalent of N_2 . When N_2 gas at $P_{\text{N}_2} = 100$ kPa was loaded at

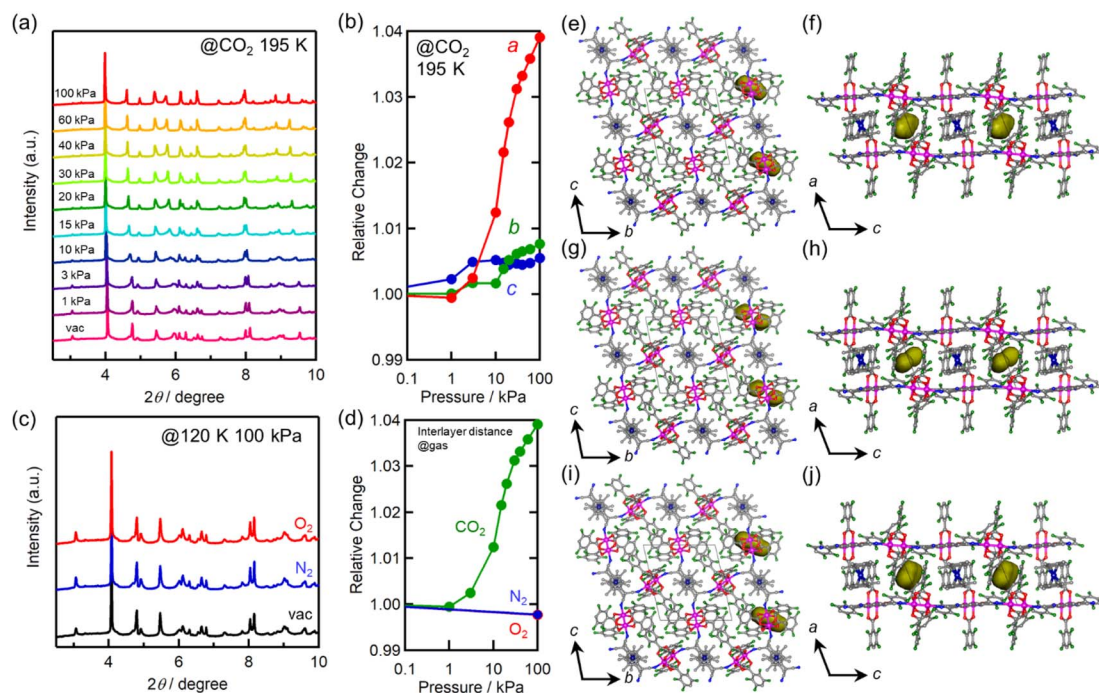


Fig. 4 Structural changes of **1** upon gas adsorption. (a) CO_2 -pressure dependence of PXRD patterns measured at 195 K. (b) Relative changes in the a -, b -, and c -axes at 195 K as a function of CO_2 pressure, where the values were normalized by the value under vacuum. (c) PXRD patterns at $P_{\text{gas}} = 100$ kPa of O_2 and N_2 and at 120 K. (d) The gas-pressure dependence of relative change of the a -axis for each gas. (e and f) Packing views of $\mathbf{1} \supset \text{O}_2$ projected along the a - and b -axes, respectively. (g and h) Packing views of $\mathbf{1} \supset \text{CO}_2$ projected along the a - and b -axes, respectively. (i and j) Packing views of $\mathbf{1} \supset \text{CO}_2$ projected along the a - and b -axes, respectively. In the figures of (e–j), hydrogen atoms are omitted for clarity; C, N, Co, and Ru atoms are presented in gray, blue, navy, and purple, respectively and Connolly surfaces that would be shared by accommodated gas molecules are shown in yellow.



120 K, an adsorption equilibrium was reached to produce $1 \supset N_2$. While this situation was maintained in a homemade cell at MPMS (Quantum Design Ltd.),⁴⁶ the field-cooled magnetization (FCM) was measured under a magnetic field of 100 Oe ($= H$) (blue plot in Fig. 5a). The $1 \supset N_2$ phase showed a cusp of FCM at 68 K (T_N), indicating that it was still an AF. However, the T_N of $1 \supset N_2$ decreased slightly in relation to that of 1 ($\Delta T_N = 7$ K). Hence, 1 was affected by N_2 accommodation, but not significantly. The magnetic field dependence of the FCM curves of $1 \supset N_2$ exhibited characteristics of metamagnetism,⁵⁴ showing a spin flip in the H range of 500–600 Oe (Fig. S3a†). This metamagnetic behavior was confirmed by varying the applied magnetic field (H) at a fixed temperature, where the initial M curve clearly displayed a spin-flipping phenomenon upon magnetic field sweeping (M - H curve, Fig. 5b and S3b†), easily recognizable in the dM/dH vs. H plots (Fig. S3c†). A H - T magnetic phase diagram was prepared based on these results (Fig. 5d). The H - T area of the AF phase in $1 \supset N_2$ was smaller than that in 1 . Although the AF phase of $1 \supset N_2$ was very similar to that of 1 at low temperatures such as 1.8 K, the boundary between the AF and paramagnetic (P) phases was affected by the adsorption of only one molar equivalent of N_2 . Despite $1 \supset N_2$ having the AF phase, it became a magnetic-field-induced F similar to 1 ,⁵⁴ exhibiting the same magnetic hysteresis loop (Fig. 5b), where the saturated magnetization (M_s) at 7 T was $1.1 N\mu_B$, the remnant magnetization (M_R) was $0.9 N\mu_B$, and the coercive field (H_c) was 2.35 T.

The magnetic behavior of $1 \supset O_2$ was similar to $1 \supset N_2$. O_2 gas with $P_{O_2} = 100$ kPa was loaded at 120 K to address the adsorption equilibrium of $1 \supset O_2$. In the FCM curve under $H = 100$ Oe,

a cusp of FCM was observed at $T_N = 68$ K (red plot in Fig. 5a), indicating the transition to the AF phase. The T_N of $1 \supset O_2$ was the same as that of $1 \supset N_2$. The FCM curves of $1 \supset O_2$ exhibited a spin flip in the H range of 200–300 Oe (Fig. S4a†), which was lower than those in $1 \supset N_2$, suggesting that the AF phase in $1 \supset O_2$ was more easily converted to the P phase than in $1 \supset N_2$. By evaluating the spin-flipping fields from the initial M - H curve (Fig. 5b, S4b, and c†), an H - T magnetic phase diagram was prepared, as shown in Fig. 5d. The AF phase of $1 \supset O_2$, as well as that of $1 \supset N_2$, was regarded to be essentially identical to that of 1 at low temperatures (1.8–10 K). In the temperature range from 10 K to T_N , the AF phase of $1 \supset O_2$ is more easily governed by applying magnetic fields than those of $1 \supset N_2$ and 1 , likely in the order of $1 \supset O_2 > 1 \supset N_2 > 1$. This order may be associated with the number of gas molecules accommodated.

In addition to $1 \supset N_2$, $1 \supset O_2$ is a magnetic-field-induced F with a magnetic hysteresis loop (Fig. 5b).⁵⁴ However, the M_s value at $H = 7$ T of $1 \supset O_2$ was $2.5 N\mu_B$, which is much larger than those of $1 \supset N_2$ and 1 . This is due to the paramagnetic contribution of accommodated O_2 ($S = 1$) in the pores of $1 \supset O_2$.⁴⁶ However, it should be noted that the O_2 spins could not be associated with long-range ordering mainly derived from the $[Ru_2]_2$ -TCNQ layers; rather, the paramagnetic O_2 contribution was likely superposed on the magnetic behavior of 1 .⁴³ Indeed, the value of M_R was the same ($0.9 N\mu_B$) for all compounds. The H_c of $1 \supset O_2$ was 1.95 T, which was only slightly smaller than that of 1 .

The magnetic properties of 1 under the CO_2 atmosphere were distinct from those under N_2 and O_2 atmospheres. The FCM curves of 1 were measured at $H = 100$ Oe under different

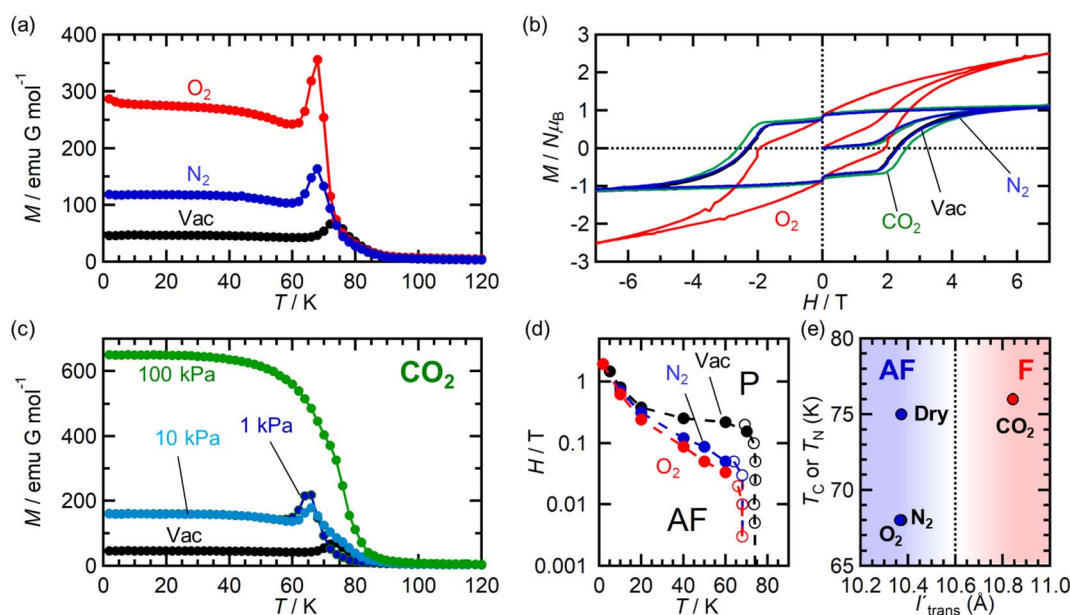


Fig. 5 Variations of magnetic properties of 1 under N_2 , O_2 , and CO_2 atmospheres. (a) FCM curves at $H = 100$ Oe for 1 measured under vacuum (black) and $1 \supset N_2$ (blue) and $1 \supset O_2$ (red) measured at $P_{\text{gas}} = 100$ kPa. (b) Magnetic hysteresis loops at 1.8 K for 1 measured under vacuum (black) and $1 \supset N_2$ (blue), $1 \supset O_2$ (red), and $1 \supset CO_2$ (green) measured at $P_{\text{gas}} = 100$ kPa. (c) CO_2 -pressure dependence of FCM curves at $H = 100$ Oe for 1 . (d) H - T phase diagrams for 1 (black), $1 \supset N_2$ (blue), and $1 \supset O_2$ (red), where AF and P represent the antiferromagnetic and paramagnetic phases, respectively. (e) Magnetic phase transition temperature (T_c or T_N) vs. I_{trans} plots for 1 and $1 \supset$ gas ($P_{\text{gas}} = 100$ kPa).



CO₂ pressure conditions ($P_{\text{CO}_2} = 1, 10, \text{ and } 100 \text{ kPa}$), after reaching adsorption equilibrium at 195 K (Fig. 5c). At $P_{\text{CO}_2} = 1$ and 10 kPa, **1** still exhibited an antiferromagnetic transition at $T_N = 68 \text{ K}$, lower than $T_N = 75 \text{ K}$ for **1** and the same as those for **1**⊃N₂ and **1**⊃O₂. However, at $P_{\text{CO}_2} = 100 \text{ kPa}$, where **1**⊃CO₂ is formed, the magnetization steeply increased at approximately 80 K and reached the maximum at 1.8 K without cusp or anomaly of FCM, indicating the onset of ferrimagnetic long-range ordering. This behavior was similarly observed even when a weak field, such as that at $H = 5 \text{ Oe}$, was applied (Fig. S5†). Hence, **1**⊃CO₂ ($P_{\text{CO}_2} = 100 \text{ kPa}$) was an F. T_C was determined to be 76 K from the M_R vs. T curve (Fig. S5†). The M - H curve of **1**⊃CO₂ at $T = 1.8 \text{ K}$ was very similar to those of **1** and **1**⊃N₂, with $M_S = 1.1 N\mu_B$, $M_R = 0.9 N\mu_B$, and $H_C = 2.62 \text{ T}$. The H_C value was slightly higher than those of the others (Fig. 5d).

Based on the magnetic properties of **1**⊃gas, the state of **1** at $P_{\text{CO}_2} \leq 10 \text{ kPa}$ could be identical to those of **1**⊃N₂ and **1**⊃O₂ ($P_{\text{N}_2/\text{O}_2} = 100 \text{ kPa}$). At higher P_{CO_2} values beyond the structural transition event at $P_{\text{CO}_2} = 15\text{--}20 \text{ kPa}$, **1**⊃CO₂ could change to achieve the F phase. This implied that the magnetic phase of **1** was directly dependent on the amount of accommodated guest, regardless of the type of gas molecule (N₂, O₂, or CO₂). Notably, all magnetic behaviors found under gases were entirely reverted to the original ones upon gas desorption by increasing the temperature to 350 K under vacuum (Fig. S6†).

Magnetic phase change upon CO₂ adsorption of **1**

Fig. 6 summarizes the possible spin alignments with a couple of magnetic interactions J_{NNI} and J_{NNNI} in the present π -PLF systems. J_{NNI} is the nearest-neighbor interaction, that is, the magnetic interaction between $[\text{MCP}_2]^{*+}$ and TCNQ⁻ radicals in

the $[\text{Ru}_2]_2$ -TCNQ layer, and J_{NNNI} is the next-nearest-neighbor interaction corresponding to the inter-layer magnetic interaction. Compound **1** showed a clear conversion from AF to F upon the complete adsorption of CO₂ at $P_{\text{CO}_2} = 100 \text{ kPa}$ (*i.e.*, **1** changed to **1**⊃CO₂), whereas **1**⊃N₂ and **1**⊃O₂ were still AFs although their phases were distinct from that of **1** with a different T_N . This change is likely due to the variation in the magnetic interaction between the two-dimensional layers J_{NNNI} because $[\text{CoCp}_2]^{*+}$ is diamagnetic (Fig. 6a and b),⁵⁴ which changes from AF to F upon CO₂ adsorption. As an empirical rule, J_{NNNI} in the family of $[\text{Ru}_2]_2$ -TCNQ layered magnets is related to l_{trans} as $l'_{\text{trans}} = l_{\text{trans}}/(\cos \psi)^{2/3}$, where ψ is the angle formed between the Ru-Ru bond and a hypothetical flat layer of the $[\text{Ru}_2]_2$ -TCNQ plane (Fig. S7†).^{32,44,64,65} When $l'_{\text{trans}} < 10.6 \text{ \AA}$, J_{NNNI} likely becomes AF.^{32,44} Table 1 summarizes the relevant parameters in the series of **1** and **1**⊃gas, and Fig. 5e shows the plots of magnetic transition temperature (T_C or T_N) vs. l'_{trans} . The l'_{trans} values of **1**, **1**⊃N₂, and **1**⊃O₂ were all 10.37 Å, while that of **1**⊃CO₂ was 10.84 Å. These relationships demonstrate that only **1**⊃CO₂ was an F (Fig. 5e). The adsorbed amount of CO₂ in **1** was higher than those of N₂ and O₂, which is a crucial reason more significant structural changes were induced only upon CO₂ adsorption (Fig. 5e). Meanwhile, **1** at $P_{\text{CO}_2} = 10 \text{ kPa}$ was still an AF, similar to **1**⊃N₂ and **1**⊃O₂ (their T_N was also identical). Thus, the structural modification involving gate-type adsorption found around $P_{\text{CO}_2} \approx 15\text{--}20 \text{ kPa}$ in the adsorption isotherm (Fig. 3) should be key for this transition. Indeed, the framework structure at $P_{\text{CO}_2} < 15 \text{ kPa}$ was identical to those of **1**⊃N₂ and **1**⊃O₂ (Fig. 4).

Here, we comment on the effect of porosity on CO₂ adsorption, which could be associated with CO₂ diffusion at a higher temperature of 195 K. Compound **1** has isolated pores (Fig. 2a and b), and even all **1**⊃gas compounds have isolated gas-accommodating pores. Thus, hopping from pore to pore is required for the gas molecules to penetrate deeply into a crystal. A high temperature, such as 195 K, could be favorable for transient structural modulations with the help of active thermal vibrations of the framework. Conversely, structural changes for hopping are unlikely to occur at low temperatures, which hinders the gas-hopping diffusion between isolated pores. For some gases at low temperatures, an adsorption equilibrium could not be reached within a practical measurement time because their gas diffusion was very slow. The O₂ adsorbed amount in **1** ($P_{\text{O}_2} = 99 \text{ kPa}$) was lower at 90 K than at 120 K, and N₂ was adsorbed at 120 K but not at 77 K (Fig. 3). In addition, the kinetic molecular radius of CO₂ (3.3 Å) is smaller than that of O₂ (3.46 Å) and N₂ (3.64 Å),⁶⁶ which also facilitates diffusion and

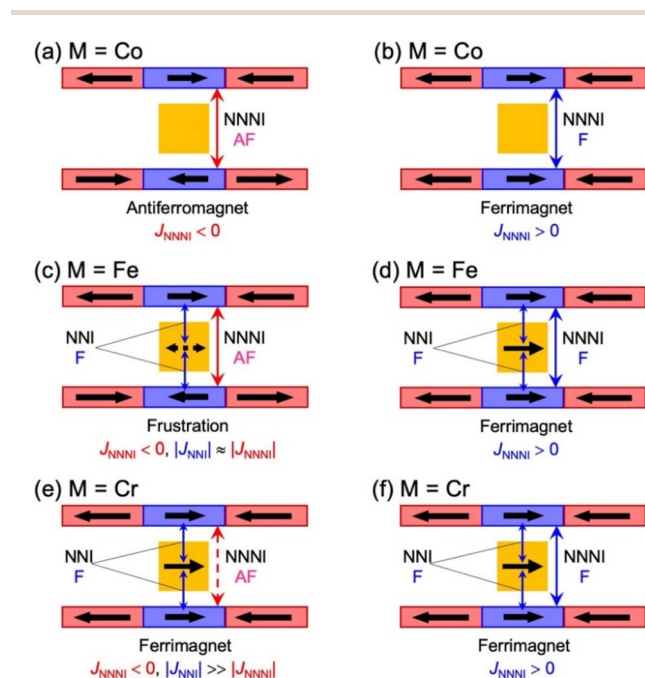


Fig. 6 Schematic representation of the possible spin alignments in the present π -PLF.

Table 1 Structural and magnetic properties of **1** and **1**⊃gas

	1	1 ⊃N ₂	1 ⊃O ₂	1 ⊃CO ₂
$l_{\text{trans}}/\text{\AA}$	10.36	10.36	10.36	10.83
$\psi/\text{deg.}$	4.9	5.9	6.1	3.9
$l'_{\text{trans}}/\text{\AA}$	10.37	10.37	10.37	10.84
T_C or T_N/K	75	68	68	76
Magnetic ground state	AF	AF	AF	F



appears as a difference in the adsorption amount. Thus, both the amount of accommodated gas molecules and the type of accommodated gas are effective in this phenomenon.

Magnetic properties of 2 and 3 under gases

Isostructural compounds 2 and 3 showed gas adsorption capabilities similar to that of 1 (Fig. 6) despite having different $[\text{MCP}_2]^{*+}$ moieties with $\text{M} = \text{Fe}$ ($S = 1/2$) and Cr ($S = 3/2$), respectively.⁵⁴ Therefore, the structural responses of 2 and 3 to gas adsorption were similar to that of 1 (details are described in the ESI†). Because only 3 has a slightly larger pore size with a larger l_{trans} ($= a$ -axis) than 1 and 2 (see the section on structures), the amounts of adsorbed gases in 3 were slightly larger than those in 1 and 2 (Fig. 3). However, 2 and 3 have additional spins of $[\text{MCP}_2]^{*+}$ with $\text{M} = \text{Fe}$ ($S = 1/2$) and Cr ($S = 3/2$), respectively, between the $[\text{Ru}_2]_2$ -TCNQ layers; therefore, J_{NNI} should be considered in addition to inter-layer interaction J_{NNNI} (Fig. 6c–f).

Fig. 7a shows the FCM curve of 2 at $H = 100$ Oe under different gas atmospheres with $P_{\text{gas}} = 100$ kPa (Fig. S13† shows the remnant magnetization (RM), zero-field-cooled magnetization (ZFCM), and FCM. Fig. S14† shows the M - T curves of 2 at $H = 5$ Oe). Due to the competition between J_{NNI} (ferromagnetic) and J_{NNNI} (antiferromagnetic), as shown in Fig. 6c, 2 underwent a transition to a spin frustration phase (FR phase) at $T_{\text{N}} = 69$ K, followed by transfer to the F phase at 44 K ($= T_{\text{R}}$) (Fig. 7a).^{54,67–70} Upon loading N_2 at $P_{\text{N}_2} = 100$ kPa and 120 K, the FCM curve followed that of 2 but continuously increased without anomaly until $T = 1.8$ K, losing the FR phase under this condition (Fig. 7a). Namely, the antiferromagnetic interaction of J_{NNNI} in 2

could be weakened by N_2 adsorption; consequently, the closest interaction J_{NNI} (ferromagnetic) for the π -contact $[\text{FeCp}_2]^{*+}$ and TCNQ moieties could be relatively dominant. The T_{C} value of 60 K was estimated for $2 \supset \text{N}_2$ from the $M_{\text{R}}-T$ curve (Fig. S13†). Meanwhile, in the M - T curve of $2 \supset \text{N}_2$ at $H = 5$ Oe, the $M_{\text{R}}-T$ curve showed a larger magnetization than the FCM curve in the temperature range of 30 – 50 K by passing through the quasi-field-induced ferrimagnetic state, indicating that the FR phase was maintained at a lower magnetic field of 5 Oe (Fig. S14a†). The behavior of “decreasing of the FR phase” was also seen for $2 \supset \text{O}_2$, in which T_{C} was identical to that of $2 \supset \text{N}_2$.

At first glance, the magnetic behavior of $2 \supset \text{CO}_2$ appeared to be similar to those of $2 \supset \text{N}_2$ and $2 \supset \text{O}_2$ but was expected to have an F phase distinct from those of $2 \supset \text{N}_2$ and $2 \supset \text{O}_2$ (Fig. 7a). The T_{C} of $2 \supset \text{CO}_2$ was 64 K, higher than that of $2 \supset \text{N}_2$ and $2 \supset \text{O}_2$. Instead, the whole feature of FCM in $2 \supset \text{CO}_2$, representing the effect of CO_2 accommodation in 2, was similar to that found in $1 \supset \text{CO}_2$. Considering the similarity of the structure and gas adsorption capability between 1 and 2, J_{NNNI} in $2 \supset \text{CO}_2$ and $1 \supset \text{CO}_2$ were completely altered to ferromagnetic from antiferromagnetic in 1 and 2 (Fig. 6d).

The M - H curves of all $2 \supset \text{gas}$ compounds were measured at 1.8 K (Fig. S15a†). The shape of the hysteresis loops was similar to that in 2, in which the anisotropic paramagnetic spin of $[\text{FeCp}_2]^{*+}$ was closely associated with the sigmoidal shape of spin flipping.^{54,71} In $2 \supset \text{O}_2$ and $1 \supset \text{O}_2$, the M_{s} values were larger than the others owing to the contributions from the paramagnetic spins of the adsorbed O_2 molecules without involvement from the long-range magnetic ordering. The hysteresis loop in $2 \supset \text{CO}_2$ was slightly modified with $M_{\text{R}} = 0.90 N\mu_{\text{B}}$ and $H_{\text{c}} = 1.76$ T, proving that the state of the F phase in $2 \supset \text{CO}_2$ was different from those in $2 \supset \text{N}_2$ and $2 \supset \text{O}_2$.

Fig. 7b shows the FCM curves of 3 recorded under different gases. Two types of cases exist on the spin alignment of pristine 3; because the contribution of J_{NNNI} (< 0) should be much smaller than that of J_{NNI} (> 0) (Fig. 6e), or because both key exchanges of J_{NNNI} and J_{NNI} basically induced ferromagnetism (Fig. 6f), 3 could be considered an F with $T_{\text{C}} = 70$ K.^{54,72} As expected, $3 \supset \text{N}_2$ and $3 \supset \text{O}_2$ showed FCM curves similar to those of 3, and a noticeable qualitative change in T_{C} was not observed. However, in $3 \supset \text{CO}_2$, T_{C} became slightly higher ($T_{\text{C}} = 78$ K, from RM, Fig. S16 and S17†). The M - H curves measured at 1.8 K under N_2 and CO_2 were very similar to those of 3, which displayed a distorted hysteresis loop originating from the magnetic anisotropy of $[\text{CrCp}_2]^{*+}$ (Fig. S15b†).⁵⁴ Only $3 \supset \text{O}_2$ revealed an O_2 -paramagnetic character superposed in 3. In addition to pristine 3, the closest ferromagnetic interaction $J_{\text{NNI}} > 0$ between the spin of $[\text{CrCp}_2]^{*+}$ ($S = 3/2$) and the TCNQ moieties of the $[\text{Ru}_2]_2$ -TCNQ ferrimagnetic layers governed long-range magnetic ordering even under the gases.⁵⁴ Therefore, due to $|J_{\text{NNI}}| \gg |J_{\text{NNNI}}|$, the J_{NNNI} could always be virtually ferromagnetic although some frustration with $J_{\text{NNNI}} < 0$ (antiferromagnetic) likely occurred in the case of Fig. 6e. Interestingly, although the l_{trans} distance in $3 \supset \text{CO}_2$ was longer than that in 3, the T_{C} of $3 \supset \text{CO}_2$ shifted to a higher temperature. This implied that the sign of J_{NNNI} in 3 could be negative (antiferromagnetic); however, its much smaller value compared to J_{NNI} in competing

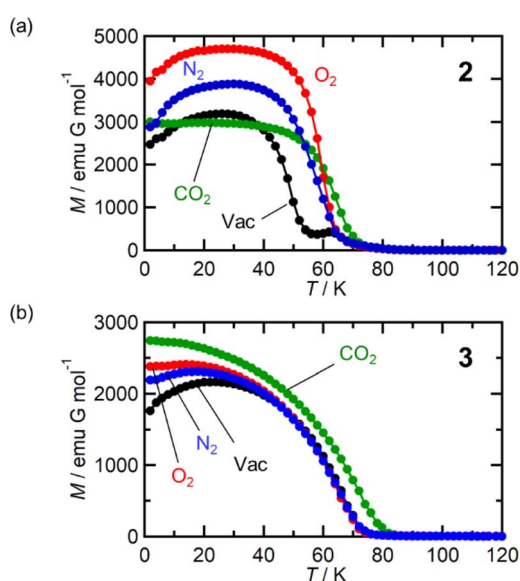


Fig. 7 Variation of magnetic properties of 2 and 3 under gases N_2 , O_2 , and CO_2 . (a) FCM curves of 2 at $H = 100$ Oe measured under vacuum (black) and $2 \supset \text{N}_2$ (blue), $2 \supset \text{O}_2$ (red), and $2 \supset \text{CO}_2$ (green) at $P_{\text{gas}} = 100$ kPa. (b) FCM curves of 3 at $H = 100$ Oe measured under vacuum (black) and $3 \supset \text{N}_2$ (blue), $3 \supset \text{O}_2$ (red), and $3 \supset \text{CO}_2$ (green) at $P_{\text{gas}} = 100$ kPa.



contributions suggested that **3** was an F (Fig. 6e). Thus, the insertion of CO₂ into **3** converted the antiferromagnetic J_{NNNI} in the original **3** into ferromagnetic J_{NNNI} (>0) in **3**⊃CO₂ (Fig. 6f), which produced an F of **3**⊃CO₂ with a higher T_{C} (Fig. 7b).

Conclusions

An efficient and straightforward strategy for ON/OFF switching of the magnetic ground state (*i.e.*, magnetic phase) is to invert the sign of the inter-layer magnetic interaction in a layered magnet. The inter-layer magnetic interaction is commonly associated with the inter-layer distance and the stacking modes that define the inter-layer environment. In this study, we demonstrated that the magnetic phase changes were possible by *in situ* tuning of the inter-layer distance using common gases such as CO₂, O₂, and N₂. In particular, **1** revealed a drastic magnetic phase change from an AF to F in **1**⊃CO₂ without a change in the charge-ordered state although **1**⊃N₂ and **1**⊃O₂ were still AFs but different from pristine **1**. These results confirm that the magnetic phase can be tuned by the types of gas accommodated even when common gases are used.

All common-gas-responsive porous magnets reported so far have been limited to being “magnet erasing,” which includes a change from an F to AF upon gas adsorption.^{43,46} The present work especially offers the first example of a change from an AF to F depending on the type of gas. The sign of the inter-layer magnetic interaction (J_{NNNI}) *vs.* the inter-layer distance (l_{trans} or l'_{trans}) is in good agreement with the empirical rule for the selected series of [Ru₂]₂-TCNQ layered magnets.^{32,44,64,65} Therefore, it is concluded that the phase change phenomenon described in this work originates purely from structural modification. The key factor for this mechanism is the presence of anisotropic combinations in the magnetic interactions, such as strong intralayer spin couplings and weak inter-layer dipole interactions based on low-dimensional layered systems. The latter contribution is a variable parameter that enables tuning of not only the magnitude of the interaction but also the sign of the exchange required for bulk phase changes. In other words, gas molecules, even common gases, act as good tools to modify the inter-layer dipole interactions. Hence, not only the [Ru₂]₂-TCNQ systems but also other families of porous layered AFs with strong intralayer and weak inter-layer interactions could be promising candidates for magnetic switching *via* similar mechanisms.

Data availability

All data supporting the findings of this study, including the details of the experimental study, are available in the article and ESI.†

Author contributions

W. K. and H. M. conceived the study. H. N. and K. N. prepared and characterized the materials. W. K., H. N., and K. N. recorded the PXRD data at the laboratory level, and S. K. and K. S. recorded the PXRD data using a synchrotron X-ray beam at the

Super Photon ring (Spring-8). W. K., H. N., and K. N. carried out the experiments of gas adsorption, *in situ* IR spectroscopy, and *in situ* gas adsorption–magnetic measurements. W. K. analyzed the structures of **1** and **1**⊃gas using Rietveld refinement techniques by using synchrotron PXRD data. H. M. supervised all the experiments. W. K. and H. M. prepared the original draft, and all authors discussed the results and commented on the manuscript.

Conflicts of interest

There are no conflicts to declare.

Acknowledgements

This work was financially supported by a Grant-in-Aid for Scientific Research (No. 18H05208, 20H00381, 21H01900, 21K18925) from MEXT, Japan; the GIMRT program; and the E-IMR project, Tohoku University, and Noguchi Institute (W. K.).

Notes and references

- G. M. Espallargas and E. Coronado, *Chem. Soc. Rev.*, 2018, **47**, 533–557.
- A. E. Thorarinsdottir and T. D. Harris, *Chem. Rev.*, 2020, **120**, 8716–8789.
- E. Coronado and G. M. Espallargas, *Chem. Soc. Rev.*, 2013, **42**, 1525–1539.
- P. Dechambenoit and J. R. Long, *Chem. Soc. Rev.*, 2011, **40**, 3249–3265.
- M. Kurmoo, *Chem. Soc. Rev.*, 2009, **38**, 1353–1379.
- S. Ohkoshi, A. Namai and H. Tokoro, *Coord. Chem. Rev.*, 2019, **380**, 572–583.
- D. A. Reed, B. K. Keitz, J. Oktawiec, J. A. Mason, T. Runčevski, D. J. Xiao, J. E. Darago, V. Crocellà, S. Bordiga and J. R. Long, *Nature*, 2017, **550**, 96–100.
- S. Kitagawa, R. Kitaura and S. Noro, *Angew. Chem., Int. Ed.*, 2004, **43**, 2334–2375.
- O. M. Yaghi, M. O’Keeffe, N. W. Ockwig, H. K. Chae, M. Eddaoudi and H. Kim, *Nature*, 2003, **423**, 705–714.
- T. R. Cook, Y.-R. Zheng and P. J. Stang, *Chem. Rev.*, 2013, **113**, 734–777.
- R. A. Potyrailo, *Chem. Rev.*, 2016, **116**, 11877–11923.
- I. Stassen, N. Burtch, A. Talin, P. Falcaro, M. Allendorf and R. Ameloot, *Chem. Soc. Rev.*, 2017, **46**, 3185–3241.
- H. Li, L. Li, R.-B. Ln, W. Zhou, Z. Zhang, S. Xiang and B. Chen, *EnergyChem*, 2019, **1**, 100006.
- L. E. Kreno, K. Leong, O. K. Farha, M. Allendorf, R. P. Van Duyne and J. T. Hupp, *Chem. Rev.*, 2012, **112**, 1105–1125.
- P. Silva, S. M. F. Viela, J. P. C. Tomé and F. A. A. Paz, *Chem. Soc. Rev.*, 2015, **44**, 6774–6803.
- O. Kahn, *Molecular Magnetism*, VCH Publishers, Inc., 1993.
- E. Coronado, *Nat. Rev. Mater.*, 2020, **5**, 87–104.
- J. S. Miller, *Chem. Soc. Rev.*, 2011, **40**, 3266–3296.
- J. Ferrando-Soria, J. Vallejo, M. Castellano, J. Martínez-Lillo, E. Pardo, J. Cano, I. Castro, F. Lloret, R. Ruiz-García and M. Julve, *Coord. Chem. Rev.*, 2017, **339**, 17–103.



- 20 B. Sieklucka and D. Pinkowicz, *Molecular Magnetic Materials, Concept and Applications*, Wiley-VCH, Verlag GmbH & Co., KGaA, Weinheim, 2017.
- 21 J. G. Park, B. A. Collins, L. E. Darago, T. Runčevski, M. E. Ziebel, M. L. Aubrey, H. Z. H. Jiang, E. Velasquez, M. A. Green, J. D. Goodpaster and J. R. Long, *Nat. Chem.*, 2021, **13**, 594–598.
- 22 C. M. Wynn, M. A. Girtu, W. B. Brinckerhoff, K. Sugiura, J. S. Miller and A. J. Epstein, *Chem. Mater.*, 1997, **9**, 2156–2163.
- 23 H. Kurebayashi, J. H. Garcia, S. Khan, J. Sinova and S. Roche, *Nat. Rev. Phys.*, 2022, **4**, 150–166.
- 24 B. Huang, G. Clark, E. Navarro-Moratalla, D. R. Klein, R. Cheng, K. L. Seyler, D. Zhong, E. Schmidgall, M. A. McGuire, D. H. Cobden, W. Yao, D. Xiao, P. Jarillo-Herrero and X. Xu, *Nature*, 2017, **546**, 270–273.
- 25 X. Zhang, Q. Lu, W. Liu, W. Niu, J. Sun, J. Cook, M. Vaninger, P. F. Miceli, D. J. Singh, S.-W. Lian, T.-R. Chang, X. He, J. Du, He. Liang, R. Zhang, G. Bian and Y. Xu, *Nat. Commun.*, 2021, **12**, 2492.
- 26 P. Perlepe, I. Oyarzabal, A. Mailman, M. Yquel, M. Platonov, I. Dovgaliuk, M. Rouzières, P. Négier, D. Mondieig, E. A. Sutura, M.-A. Dourges, S. Bonhommeau, R. A. Musgrave, K. S. Pedersen, D. Chernyshov, F. Wilhelm, A. Rogalev, C. Mathonière and R. Clérac, *Science*, 2020, **370**, 587–592.
- 27 C. Gong, L. Li, Z. Li, H. Ji, A. Stern, Y. Xia, T. Cao, W. Bao, C. Wang, Y. Wang, Z. Q. Qiu, R. J. Cava, S. G. Louie, J. Xia and X. Zhang, *Nature*, 2017, **546**, 265–269.
- 28 K. S. Burch, D. Mandrus and J.-G. Park, *Nature*, 2018, **563**, 47–52.
- 29 S. Jiang, J. Shan and K. F. Mak, *Nat. Mater.*, 2018, **17**, 406–410.
- 30 B. Li, Z. Wan, C. Wang, P. Chen, B. Huang, X. Cheng, Q. Qian, J. Li, Z. Zhang, G. Sun, B. Zhao, H. Ma, R. Wu, Z. Wei, Y. Liu, L. Liao, Y. Ye, Y. Huang, X. Xu, X. Duan, W. Ji and X. Duan, *Nat. Mater.*, 2021, **20**, 818–825.
- 31 W.-B. Zhang, Q. Qu, P. Zhu and C.-H. Lam, *J. Mater. Chem. C*, 2015, **3**, 12457–12468.
- 32 H. Miyasaka, *Acc. Chem. Res.*, 2013, **46**, 248–257.
- 33 H. Miyasaka, *Bull. Chem. Soc. Jpn.*, 2021, **94**, 2929–2955.
- 34 D. MasPOCH, D. Ruiz-Molina, K. Wurst, N. Domingo, M. Cavallini, F. Biscarini, J. Tejada, C. Rovira and J. Veciana, *Nat. Mater.*, 2003, **2**, 190–195.
- 35 W. Kaneko, M. Ohba and S. Kitagawa, *J. Am. Chem. Soc.*, 2007, **129**, 13706–13712.
- 36 N. Motokawa, S. Matsunaga, S. Takaishi, H. Miyasaka, M. Yamashita and K. R. Dunbar, *J. Am. Chem. Soc.*, 2010, **132**, 11943–11951.
- 37 I. Jeon, B. Negru, R. P. V. Duyne and T. D. Harris, *J. Am. Chem. Soc.*, 2015, **137**, 15699–15702.
- 38 M. Wriedt, A. A. Yakovenko, G. J. Halder, A. V. Prosvirin, K. R. Dunbar and H.-C. Zhou, *J. Am. Chem. Soc.*, 2013, **135**, 4040–4050.
- 39 D. Pinkowicz, R. Podgajny, B. Gawel, W. Nitek, W. Łasocha, M. Oszejca, M. Czaplá, M. Makarewicz, M. Bálánda and B. Sieklucka, *Angew. Chem., Int. Ed.*, 2011, **50**, 3973–3977.
- 40 H. Yoshino, N. Tomokage, A. Mishima, B. Le Ouay, R. Ohtani, W. Kosaka, H. Miyasaka and M. Ohba, *Chem. Commun.*, 2021, **57**, 5211–5214.
- 41 J. Zhang, W. Kosaka, K. Sugimoto and H. Miyasaka, *J. Am. Chem. Soc.*, 2018, **140**, 5644–5652.
- 42 J. Zhang, W. Kosaka, Y. Kitagawa and H. Miyasaka, *Angew. Chem., Int. Ed.*, 2019, **58**, 7351–7356.
- 43 J. Zhang, W. Kosaka, Y. Kitagawa and H. Miyasaka, *Nat. Chem.*, 2021, **13**, 191–199.
- 44 J. Zhang, W. Kosaka, H. Sato and H. Miyasaka, *J. Am. Chem. Soc.*, 2021, **143**, 7021–7031.
- 45 J. Chen, Y. Sekine, A. Okazawa, H. Sato, W. Kosaka and H. Miyasaka, *Chem. Sci.*, 2020, **11**, 3610–3618.
- 46 W. Kosaka, Z. Liu, J. Zhang, Y. Sato, A. Hori, R. Matsuda, S. Kitagawa and H. Miyasaka, *Nat. Commun.*, 2018, **9**, 5420.
- 47 J. Zhang, W. Kosaka, Y. Kitagawa and H. Miyasaka, *Angew. Chem., Int. Ed.*, 2022, **61**, e202115976.
- 48 J. A. R. Navarro, E. Barea, A. Todriuez-Diéguéz, J. M. Salas, C. O. Ania, J. B. Parra, N. Masciocchi, S. Galli and A. Sironi, *J. Am. Chem. Soc.*, 2008, **130**, 3978–3984.
- 49 S. S. Kaye, H. J. Choi and J. R. Long, *J. Am. Chem. Soc.*, 2008, **130**, 16921–16925.
- 50 M. Kurmoo, H. Kumagai, K. W. Chapman and C. J. Kepert, *Chem. Commun.*, 2005, 3012–3014.
- 51 S. Ohkoshi, Y. Tsunobuchi, H. Takahashi, T. Hozumi, M. Shiro and K. Hahimoto, *J. Am. Chem. Soc.*, 2007, **129**, 3084–3085.
- 52 Y. Yoshida, K. Inoue, K. Kikuchi and M. Kurmoo, *Chem. Mater.*, 2016, **28**, 7029–7038.
- 53 H. Fukunaga and H. Miyasaka, *Angew. Chem., Int. Ed.*, 2015, **54**, 569–573.
- 54 H. Fukunaga, W. Kosaka, H. Nemoto, K. Taniguchi, S. Kawaguchi, K. Sugimoto and H. Miyasaka, *Chem.-Eur. J.*, 2020, **26**, 16755–16766.
- 55 G. A. Candela, L. J. Swartzendruber, J. S. Miller and M. J. Rice, *J. Am. Chem. Soc.*, 1979, **101**, 2755–2756.
- 56 J. S. Miller, A. H. Reis Jr, E. Gebert, J. J. Ritsko, W. R. Salaneck, L. Kovnat, T. W. Cape and R. P. Van Duyne, *J. Am. Chem. Soc.*, 1979, **101**, 7111–7113.
- 57 J. S. Miller, J. H. Zhang, W. M. Reiff, D. A. Dixon, L. D. Preston, A. H. Reis, E. Gebert, M. Extine, J. Troup, A. J. Epstein and M. D. Ward, *J. Phys. Chem.*, 1987, **91**, 4344–4360.
- 58 W. E. Broderick and B. M. Hoffman, *J. Am. Chem. Soc.*, 1991, **113**, 6334–6335.
- 59 W. E. Broderick, D. M. Eichhorn, X. Liu, P. J. Toscano, S. M. Owens and B. M. Hoffman, *J. Am. Chem. Soc.*, 1995, **117**, 3641–3642.
- 60 S. H. Lapidus, P. W. Stephens, M. Fumanal, J. Ribas-Ariño, J. J. Novoa, J. G. DaSilva, A. L. Rheingold and J. S. Miller, *Dalton Trans.*, 2021, **50**, 11228–11242.
- 61 W. Kosaka, K. Yamagishi, H. Yoshida, R. Matsuda, S. Kitagawa, M. Takata and H. Miyasaka, *Chem. Commun.*, 2013, **49**, 1594–1596.
- 62 W. Kosaka, K. Yamagishi, A. Hori, H. Sato, R. Matsuda, S. Kitagawa, M. Takata and H. Miyasaka, *J. Am. Chem. Soc.*, 2013, **135**, 18469–18480.



- 63 R. Matsuda, T. Tsujino, H. Sato, Y. Kubota, K. Morishige, M. Takata and S. Kitagawa, *Chem. Sci.*, 2010, **1**, 315–321.
- 64 W. Kosaka, M. Itoh and H. Miyasaka, *Mater. Chem. Front.*, 2018, **2**, 497–504.
- 65 W. Kosaka, Z. Liu and H. Miyasaka, *Dalton Trans.*, 2018, **47**, 11760–11768.
- 66 C. R. Reid and K. M. Thomas, *Langmuir*, 1999, **15**, 3206–3218.
- 67 J. S. Miller, A. J. Epstein and W. M. Reiff, *Chem. Rev.*, 1988, **88**, 201–220.
- 68 P. Bak and J. von Boehm, *Phys. Rev. B: Condens. Matter Mater. Phys.*, 1980, **21**, 5297–5308.
- 69 T. Kimura, S. Ishihara, H. Shintani, T. Arima, K. T. Takahashi, K. Ishizawa and Y. Tokura, *Phys. Rev. B: Condens. Matter Mater. Phys.*, 2003, **68**, 060403.
- 70 R. A. dos Anjos, J. R. Viana, J. R. de Sousa and J. A. Plascak, *Phys. Rev. E: Stat., Nonlinear, Soft Matter Phys.*, 2007, **76**, 022103.
- 71 D. N. Hendrickson, Y. S. Sohn and H. B. Gray, *Inorg. Chem.*, 1971, **10**, 1559–1563.
- 72 A. S. Nikolay, A. P. Nikolay, V. L. Anton, S. B. Artem, A. P. Elena, A. S. Elizveta, P. G. Nina, P. N. K. Sergey, M. Ruediger, I. O. Victor and V. Z. Andrey, *Inorg. Chem.*, 2010, **49**, 7558–7564.

